

# $\nu_\alpha e \rightarrow \nu_\beta e$ Aspirant for New Physics

Abrar Ahmad

*Department of Physics, COMSATS Institute of Information Technology,  
Islamabad, Pakistan. E-mail:smart5733@gmail.com*

Shakeel Mahmood

*Department of Physics, Air University, PAF Complex, E-9,  
Islamabad, Pakistan: E-mail:shakeel.mahmood@mail.au.edu.pk*

Farida Tahir

*Department of Physics, COMSATS Institute of Information Technology,  
Islamabad, Pakistan. E-mail: farida\_tahir@comsats.edu.pk*

This work focuses on the topical survey of precision measurements via  $\nu_\alpha e \rightarrow \nu_\beta e$  scattering in the frame work of Non-Standard Interaction (NSI). Both Model Independent (MI) and Model Dependent (MD) are used in addition the Standard Model (SM). R-parity violating Supersymmetry ( $\mathcal{R}_p$  SUSY) Model is used to perform MD analysis, where the scattering cross-section is influenced by new S-bosons. By using LSND experimental value, we obtain limits for  $\lambda_{1j1}$  and obtain physically allowed and disallowed regions rather than just limits/bounds for  $(\xi_{ee}^{eL}, \xi_{ee}^{eR})$ . Under the limits of CHARM-II, BNL-COL and BNL-E734 experimental values, we get physically allowed and disallowed regions for MI and MD couplings parameters  $(\xi_{\mu\mu}^{eL}, \xi_{\mu\mu}^{eR})$  and  $(\lambda_{21k}, \lambda_{2j1})$ . Sensitivity of these coupling parameters with each other is also discussed. Furthermore, we establish a relation between MI coupling parameters  $(\xi_{\alpha\beta}^{eL}, \xi_{\alpha\beta}^{eR})$  and R-parity violating SUSY Model coupling parameters  $(\lambda_{\alpha 1k}, \lambda_{\alpha j1})$ .

Keywords: Non-Standard Interaction (NSI), Model Dependent, Model Independent, SUSY, MSSM, FCNC

PACS: 12.60.-i, 13.15.+g, 13.20.-v

## I. INTRODUCTION

Current precision demands a complete understanding of model parameters in addition to their mapping with respect to experimental results. To achieve this, all the possible theoretical information for the interpretation of data is incorporated [1–3]. The compatibility between experimental data and theoretical model is only valid within the limits of experimental uncertainties.

SM treats neutrinos as massless particles, that fortifies the fact that not only lepton number and flavor will be conserved, but also  $W^\pm, Z$  weak gauge bosons universally couple with all three families of leptons [4, 5]. Contrary to that, Sudbury Neutrino Observatory (SNO) observed the flavor changing for  $^8B$  solar neutrinos, during their flight from the center of the sun to the earth [6]. Super-Kamiokande (SK) observed two-flavor  $\nu_\mu \longleftrightarrow \nu_\tau$  atmospheric neutrino oscillations [7–10]. Kamioka Liquid Scintillator Anti neutrino Detector (KamLAND), KEK to Kamioka (K2K), Main Injector Neutrino Oscillation Search (MINOS) and Mini Booster Neutrino Experiment (MiniBooNE) have measured different neutrino oscillation parameters with extraordinary precision [11]. In solar and atmospheric neutrino experiments, lepton flavour violation has been observed [3]. These evidences of neutrino oscillations implies finite neutrinos masses and mixing [12].

In the light of these facts, it is clearly established fact that there was something wrong with the naive SM description of neutrino properties at the very fundamental level. Therefore, SM either needs to be modified or extended to incorporate new interactions i.e. Non-Standard Interaction (NSI). Such a model can be possible beyond the SM that distinguish among the three generations of neutrinos, and violate neutral current universality via the direct exchange of new particles between the neutrinos and matter particles [13–33]. So, many extensions (new physics models (NPM)) of the SM with non-minimal Higgs bosons are available in the form of see-saw models, Left- Right symmetric, GUTs, 331 models and Minimal Super Symmetric Standard Model (MSSM) [11, 34–40] capable to accommodate neutrino masses in the natural way and predicting NSI at the same time.

In MSSM, operators that carry the same Baryon number ( $B$ ) and Lepton number ( $L$ ) of the SM but different spin and mass, also violate  $B$  and  $L$  conservation, which have dangerous impact on the low energy phenomenology. In particular, it means that matter is unstable due to the proton decay. To cope with this problem an ad hoc discrete symmetry namely R-parity ( $R_p = (-1)^{3B+L+2S}$ ) introduced, with  $B, L$  and intrinsic spin ( $S$ ) of the particle. Under this condition  $L$  and  $B$  number violating processes are prohibited thus preventing proton from decay [41]. As R-parity is not the demand of gauge symmetry, renormalization and anomaly free condition. Therefore in order to extend the SM, and study Beyond the SM, the possibility of B and/or L-violation must be encountered. As

an alternate solution of rapid proton decay problem, relaxed  $R_p$  conservation by assuming  $B$ -conservation but  $L$ -violation. This alleviation allowed the Yukawa couplings  $\lambda_{ijk}$  ( $LLE$ ),  $\lambda'_{ijk}$  ( $LQD$ ), their product ( $\lambda_{ijk}\lambda_{\alpha\beta\gamma}$ ,  $\lambda'_{ijk}\lambda'_{\alpha\beta\gamma}$ ) and combinations ( $\lambda_{ijk}\lambda'_{ijk}$ ) forbidden due to simultaneous presence of  $\lambda'_{ijk}$ ,  $\lambda''_{ijk}$  ( $LQD$  and  $UDD$ ) and  $\lambda_{ijk}$ ,  $\lambda''_{ijk}$  ( $LLE$  and  $UDD$ ) in most general  $\mathbb{R}_p$  superpotential Eq.(1).

$$W_{\mathbb{R}_p} = \lambda_{[ij]k} L_i L_j e_k^c + \lambda'_{ijk} L_i Q_j d_k^c + \lambda''_{[jk]i} u_i^c d_j^c d_k^c \quad (1)$$

where  $i, j, k = (1, 2, 3)$  represents three generation of quarks and lepton chiral super fields,  $L_i, Q_i, d_i^c, d_i^c$  and  $e_i^c$ . Superscript "c" denote the charge conjugate spinor. The first two terms are responsible for the lepton number violation and last term is responsible for baryon number violation. The  $SU(2)_L$  gauge invariance demands the couplings  $\lambda_{ijk}$  to be antisymmetric in the first two indices, whereas  $SU(3)_C$  gauge invariance requires the couplings  $\lambda''_{ijk}$  to be antisymmetric in the last two indices. These conditions reduce the number of  $\mathbb{R}_p$  couplings to 45 ( $9\lambda_{ijk}, 27\lambda'_{ijk}, \text{and } 9\lambda''_{ijk}$ ) [41–46].

The  $\mathbb{R}_p$  SUSY model allows flavor changing non-standard interaction (FCNSI), flavor diagonal non-standard interaction (FDNSI) at tree level and distinguish the three flavors of neutrino in interactions via direct exchanging virtual SUSY propagator. This may explain data in a better way and enrich our understanding about neutrinos. We study such (NSI) effects both in model independent (MI) and model dependent (MD) (i.e. in  $\mathbb{R}_p$  SUSY model) way by using reaction  $\nu_\alpha e \rightarrow \nu_\beta e$  ( $\alpha = \beta = e, \mu$ ). We selected  $\nu_e e \rightarrow \nu_e e$  reaction for two reasons:

(1) *It is a reliable source for the precision measurements and*

(2) *It is the only reaction (in the history of particle physics), which can proceed through both charge and neutral current interactions and confirm (support) the gauge structure of the SM.*

Elastic scattering of electron with muon neutrino *is the simplest neutral current reaction which occurs through the exchange of  $Z^0$  boson in the frame work of SM and all the parameters (as far as the SM is concerned) of this reactions are well measured experimentally by CHARM II [47] and BNL [48] experiments.*

We have also stated the contradiction between the predictions given by the Standard Model and the observation made by Liquid Scintillator Neutrino Detector (LSND) [2], CHARM-II[47], BNL-COL[49] and BNL-E734 [48] experiments.

This paper is organized as follow: In Sec.II. we perform an analysis of total elastic scattering cross-section for  $\nu_e e$  and  $\nu_\mu e$  in the context of SM and discuss discrepancy between experiments and SM prediction. In Sec.III, we perform a detail analysis of  $\nu_\alpha e \rightarrow \nu_\beta e$  in MI way and investigate the role of NSI. We also discuss the physical allowed and disallowed regions for unknown NSI parameters and discuss the sensitivity of these parameters upon one another. In Sec.IV, we calculate MD  $\nu_e e$  and  $\nu_\mu e$  elastic scattering cross-section by using  $\mathbb{R}_p$  SUSY model and obtain physical allowed and disallowed regions on NUFD  $\mathbb{R}_p$  SUSY couplings parameters. The sensitivity of these parameters in relation to each other is also discussed. Further, a relation between MI and MD coupling parameters is also developed. Finally conclusion is discussed in Sec.V.

## II. SM CROSS-SECTION

Neutrino-Electron scattering( $\nu_\alpha e \rightarrow \nu_\beta e$ ) are the simplest of purely leptonic weak processes, which are favorable for the precision test measurement and search for physics beyond SM. These include both charge current (CC) and neutral current (NC). Both CC and NC contribute in case of electron neutrino i.e.  $\alpha = \beta = e$ , and only NC contribution in case of muon and tau neutrinos i.e.  $\alpha = \beta = \mu, \tau$  within SM[50, 51]. The Feynman diagrams of these processes are shown in Fig.(1)

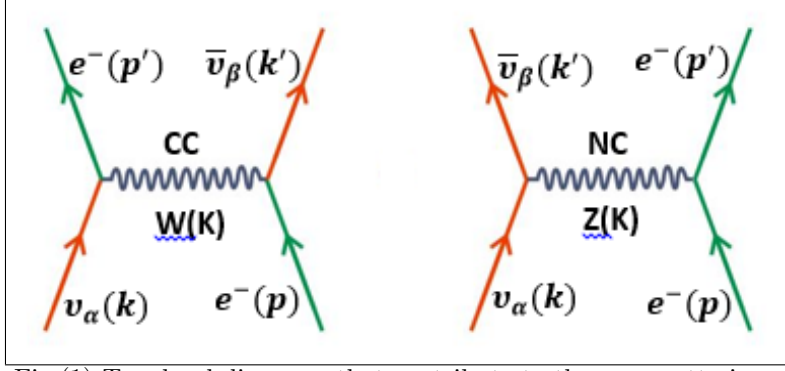


Fig.(1) Tree-level diagrams that contribute to the  $\nu_\alpha e$  scattering in the standard model [12].

In the light of SM, the effective Lagrangians of CC and NC are [52];

$${}^{CC}L_{eff} = -i2\sqrt{2}G_F[\bar{\nu}_\beta(k')\gamma_\alpha P_L\nu_\alpha(k)][\bar{e}(p')\gamma^\alpha P_L e(p)] \quad (2)$$

$${}^{NC}L_{eff} = -\sqrt{2}iG_F[\bar{\nu}_\alpha(k')\gamma_\mu P_L\nu_\alpha(k)][(\bar{e}(p')\gamma^\mu(g_L P_L + g_R P_R)e(p))] \quad (3)$$

Where  $G_F$  is Fermi coupling constant,  $P_L \equiv \left(\frac{1-\gamma^5}{2}\right)$  and  $P_R \equiv \left(\frac{1+\gamma^5}{2}\right)$  are left and right handed chiral operators respectively [52],  $g_L = g_V + g_A$ ;  $g_R = g_V - g_A$ ;  $g_V$  and  $g_A$  are vector and axial-vector coupling constants respectively. In SM,  $g_V = -\frac{1}{2} + 2\sin^2\theta_w$ ,  $g_A = -\frac{1}{2}$  and  $\sin^2\theta_w = 0.23$  is the weak mixing angle [2]. The total Lagrangian of CC and NC for  $\nu_e e \rightarrow \nu_e e$  within SM is

$$\begin{aligned} L_{SM} &= {}^{CC}L_{eff} + {}^{NC}L_{eff} \\ &= -i\sqrt{2}G_F[\bar{\nu}_e(k')\gamma_\mu P_L\nu_e(k)][\bar{e}(p')\gamma^\mu(A_L P_L + A_R P_R)e(p)] \end{aligned} \quad (4)$$

Where  $A_L \equiv 2 + g_L$  and  $A_R \equiv g_R$ . Using Eq.(4) we get the total elastic cross-section for  $\nu_e e$  as

$$\sigma_{SM}^{\nu_e e} = \sigma_o \left[ (g_L + 2)^2 + \frac{g_R^2}{3} \right] \quad (5)$$

and for  $\nu_\alpha e \rightarrow \nu_\alpha e$  ( $\alpha = \mu$ ) we get total cross-section by using Eq.(3)

$$\sigma_{SM}^{\nu_\mu e} = \sigma_o \left[ g_L^2 + \frac{g_R^2}{3} \right] \quad (6)$$

where  $\sigma_o \equiv \frac{G_F^2 m_e E_\nu}{2\pi} = 4.31 \times 10^{-45} E_\nu \text{cm}^2 / \text{Mev}$  ( $E_\nu$  is the incident energy of neutrinos). We get SM cross-section for  $\nu_e e \rightarrow \nu_e e$  and  $\nu_\mu e \rightarrow \nu_\mu e$  processes are

$$\sigma^{\nu_e e} = 9.52 \times 10^{-45} \text{cm}^2 / \text{Mev} \times E_\nu \quad (7)$$

$$\sigma^{\nu_\mu e} = 1.55 \times 10^{-45} \text{cm}^2 / \text{Mev} \times E_\nu. \quad (8)$$

The measured cross-section related to different experiments are shown in Table-I. The deviation of measured cross-section from the SM at different energies and sigma levels is shown in Figs.(2, 3, 4 and 5).

Experiment	$\sigma(\nu_e)/E_\nu \times 10^{-45} \times \text{cm}^2 \text{MeV}^{-1}$	SM Contribution	Error
LSND [2]	$10.1 \pm 1.1 \pm 1.0$	$\sim 94.3\%$	$\sim -5.7\%$
	$\sigma(\nu_\mu)/E_\nu \times 10^{-45} \times \text{cm}^2 \text{MeV}^{-1}$		
CHARM-II [47]	$1.53 \pm 0.04 \pm 0.12$	$\sim 101.6\%$	$\sim +1.6\%$
BNL-COL[49]	$1.67 \pm 0.44$	$\sim 93.1\%$	$\sim -6.9\%$
BNL-E734 [48]	$1.8 \pm 0.2 \pm 0.25$	$\sim 86.3\%$	$\sim -13.7\%$

TABLE I: Measured cross-section from different experiments and percentage SM contribution with percentage error from central value

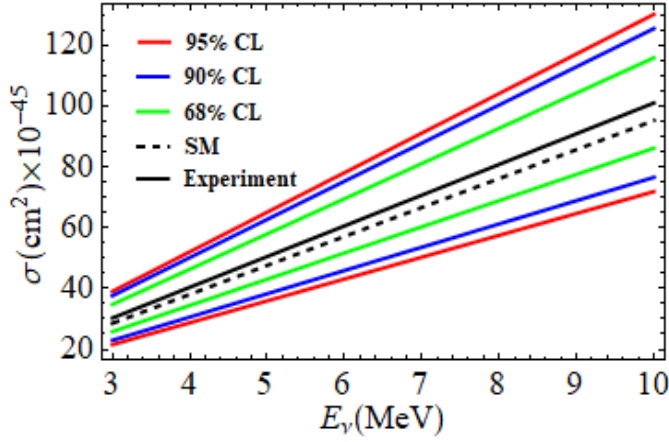


Fig.(2) Discrepancies between SM and LSND experimental cross-section for the process  $\nu_e e \rightarrow \nu_e e$  at 68%, 90% and 95% Confidence levels

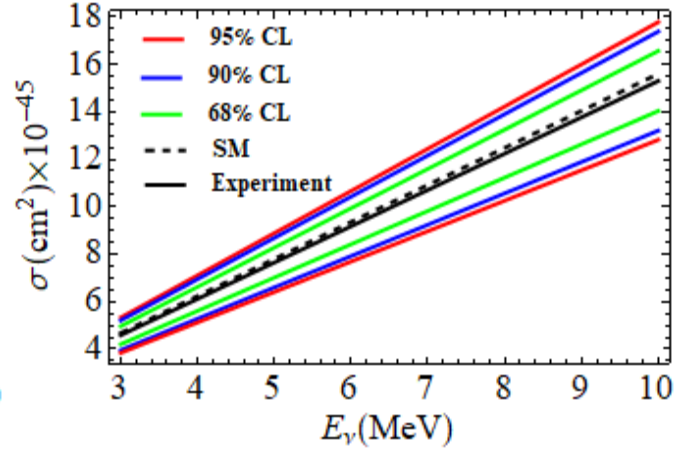


Fig.(3) Discrepancies between SM and Charm-II experimental cross-section for the process  $\nu_\mu e \rightarrow \nu_\mu e$  at 68%, 90% and 95% Confidence levels.

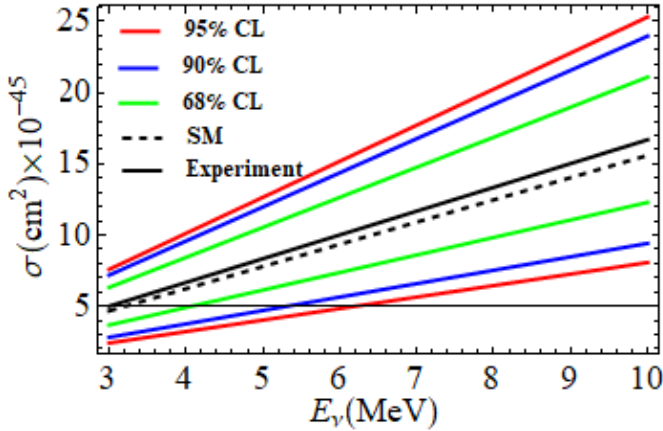


Fig.(4) Discrepancies between SM and BNL-COL experimental cross-section for the process  $\nu_\mu e \rightarrow \nu_\mu e$  at 68%, 90% and 95% Confidence levels.

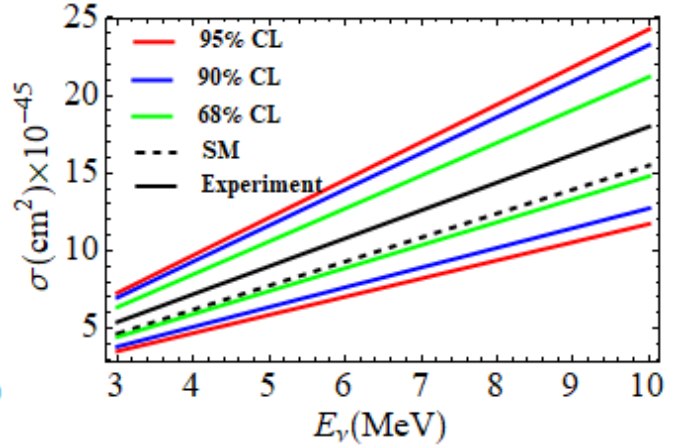


Fig.(5) Discrepancies between SM and BNL-E734 experimental cross-section for the process  $\nu_\mu e \rightarrow \nu_\mu e$  at 68%, 90% and 95% Confidence levels.

### III. MI ANALYSIS OF $\nu_\alpha e \rightarrow \nu_\beta e$

NSI play an important role in the precision of measurements. The discrepancy between the theoretical and experimental values of  $\nu_e e$  and  $\nu_\mu e$  cross-section can be accommodated by introducing NSI in terms of unknown coupling

parameters  $(\hat{\xi}_{\alpha\beta}^{eL}, \hat{\xi}_{\alpha\beta}^{eR})$ , which describe the strength of NSI. The feynman diagrams of NSI for  $\nu_\alpha e \rightarrow \nu_\beta e$  are shown in Fig.(6).

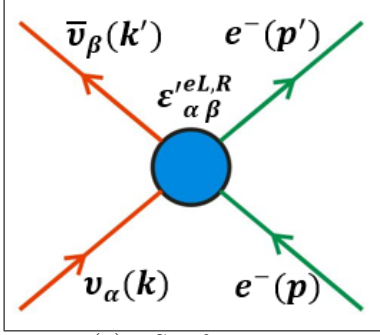


Fig.(6) NSI of neutrinos described as four-fermi interaction with new couplings [12]

The Lagrangian of Non Standard neutral current Interactions can be written as;

$$L_{(NSI)} = -\sqrt{2}iG_F [\bar{\nu}_\beta(k')\gamma_\mu P_L \nu_\alpha(k)] [\bar{e}(p')\gamma^\mu (\hat{\xi}_{\alpha\beta}^{eL} P_L + \hat{\xi}_{\alpha\beta}^{eR} P_R) e(p)] \quad (9)$$

where  $\alpha$  and  $\beta$  represent the lepton flavor ( $e, \mu$  or  $\tau$ ).  $\alpha = \beta$  represents Non Universal (NU) Flavor-conserving NSI and  $\alpha \neq \beta$  for Flavor-Changing (FC) NSI [11]. SM contributes majorly to the cross section of  $\nu_e e$  and  $\nu_\mu e$ . Therefore, NSI is considered as a sub-leading effect.

The elastic cross-section for  $\nu_e e$  and  $\nu_\mu e$  elastic cross section with contribution of NSI are given by;

$$\sigma^{v_e} = 4\sigma_o \left[ \left(1 + \frac{g_L}{2} + \hat{\xi}_{ee}^{eL}\right)^2 + \frac{1}{3} \left(\frac{g_R}{2} + \hat{\xi}_{ee}^{eR}\right)^2 \right] \quad (10)$$

$$\sigma^{v_\mu} = 4\sigma_o \left[ \left(\frac{g_L}{2} + \hat{\xi}_{\mu\mu}^{eL}\right)^2 + \frac{1}{3} \left(\frac{g_R}{2} + \hat{\xi}_{\mu\mu}^{eR}\right)^2 \right] \quad (11)$$

where  $\hat{\xi}_{\alpha\beta}^{eL,R} \equiv \frac{\xi_{\alpha\beta}^{eL,R}}{2}$  with  $(\alpha = \beta = e \text{ or } \mu)$ .

The dependency of  $\hat{\xi}_{ee}^{eR}$  to the  $\hat{\xi}_{ee}^{eL}$  can be obtain by using the LSND  $\nu_e e \rightarrow \nu_e e$  experimental value at 90% CL from Table-I in Eq.(10) as

$$\hat{\xi}_{ee}^{eR} = \pm \sqrt{\frac{3\sigma_{\text{exp}}^{v_e}}{4\sigma_o} - 3 \left(1 + \frac{g_L}{2} + \hat{\xi}_{ee}^{eL}\right)^2} - \frac{g_R}{2} \quad (12)$$

using Eq.(12), we obtained graph of allowed regions which shows sensitivity of  $\hat{\xi}_{ee}^{eR}$  on  $\hat{\xi}_{ee}^{eL}$  shown in Fig.(7a and 7b).

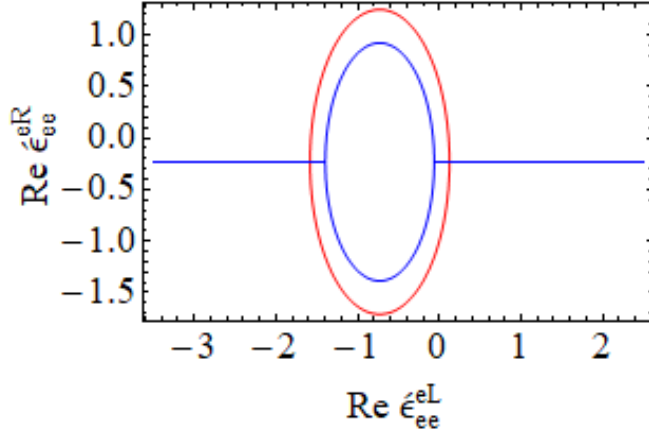


Fig.(7a) Allowed region for real part of  $\hat{\epsilon}_{ee}^{eR}$ , depends on  $\hat{\epsilon}_{ee}^{eL}$ . Blue solid line represent lower limit whereas red solid line represent upper limit of LSND experimental value at 90% CL

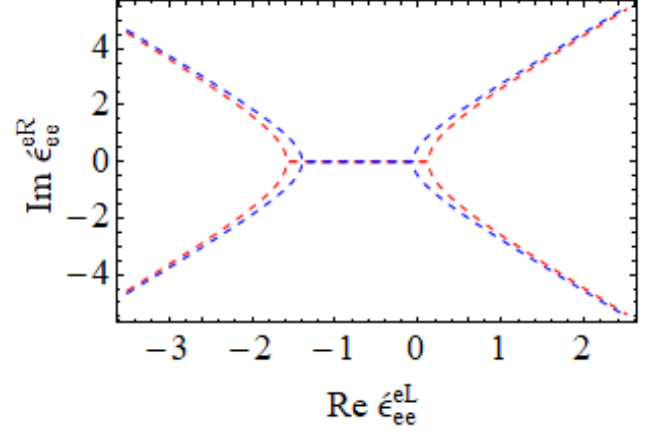


Fig.(7b) Allowed region for Imaginary part  $\hat{\epsilon}_{ee}^{eR}$ , depends on  $\hat{\epsilon}_{ee}^{eL}$ . Blue dotted line represent lower limit whereas red dotted line represent upper limit of LSND experimental value at 90% CL

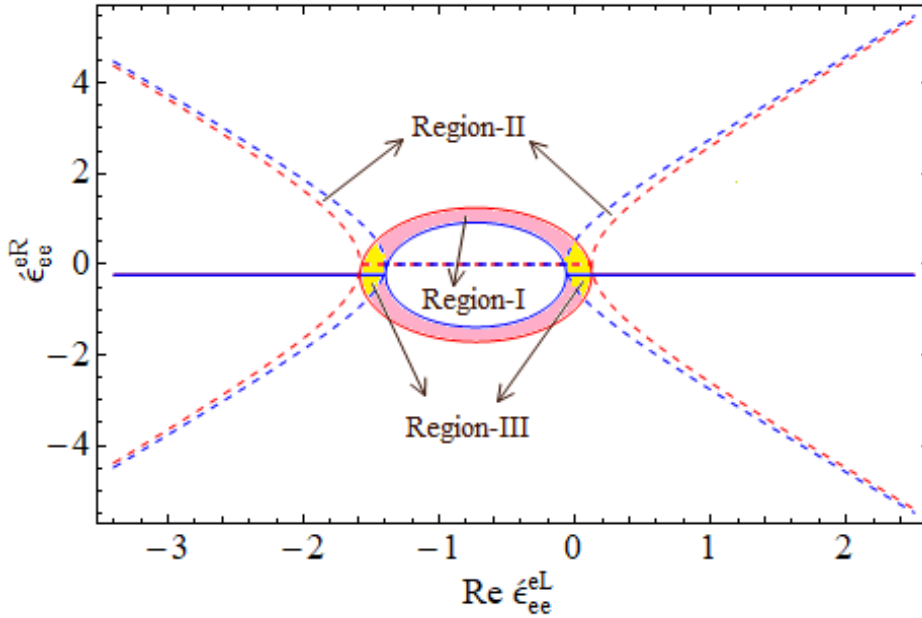


Fig.(7c) Overlapping of Figs. (7a and 7b). Region-I (Rose shaded) is real allowed for  $\hat{\epsilon}_{ee}^{eR}$ . Region-II (between red and blue dotted lines) is allowed region contain Imaginary part of  $\hat{\epsilon}_{ee}^{eR}$ , and its real part is constant represent by solid blue straight line. Region-III (yellow shaded) is allowed region contain complex  $\hat{\epsilon}_{ee}^{eR}$  (blue color) from lower limit and real  $\hat{\epsilon}_{ee}^{eR}$  (red color) from upper limit.

The overlapping of Fig.(7a) and Fig.(7b) can be seen in Fig.(7c).

In similar way we get dependency of  $\hat{\epsilon}_{\mu\mu}^{eR}$  to the  $\hat{\epsilon}_{\mu\mu}^{eL}$  by using CHARM-II, BNL-COL and BNL-E734 experimental value at 90% CL from table-1 in eq.(11) is reversed as

$$\hat{\epsilon}_{\mu\mu}^{eR} = \pm \sqrt{\frac{3\sigma_{\text{exp}}^{v\mu}}{4\sigma_o} - 3 \left( \frac{g_L}{2} + \hat{\epsilon}_{\mu\mu}^{eL} \right)^2} - \frac{g_R}{2} \quad (13)$$

By using Eq.(13), we obtained the graph of allowed regions which shows sensitivity of  $\hat{\epsilon}_{\mu\mu}^{eR}$  on  $\hat{\epsilon}_{\mu\mu}^{eL}$  shown in Fig.(9a

and 9b)

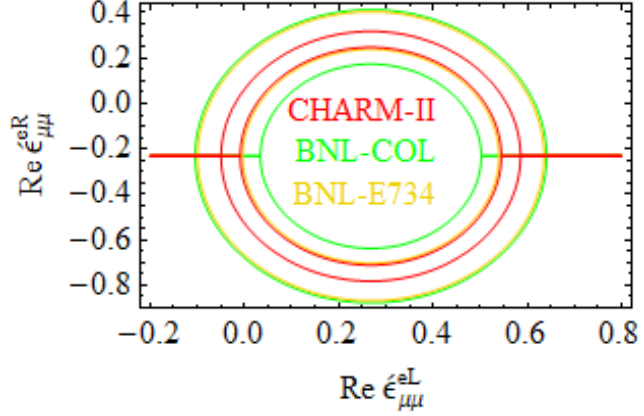


Fig.(9a) Allowed region between ellipse for real part of  $\epsilon_{ee}^{eR}$ , depends on  $\epsilon_{ee}^{eL}$ . CHARM-II, BNL-COL and BNL-E734 represented by Red, blue and orange color respectively at 90% CL

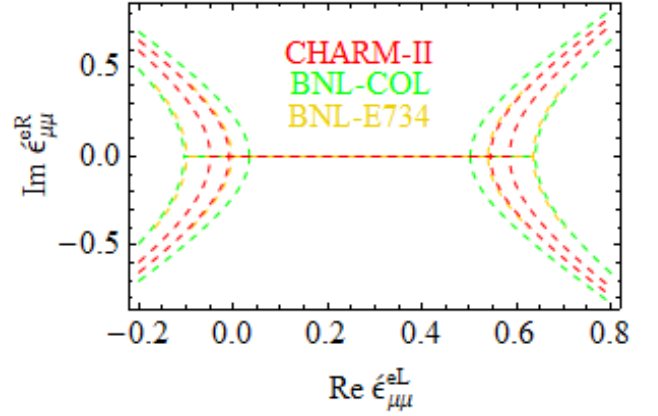
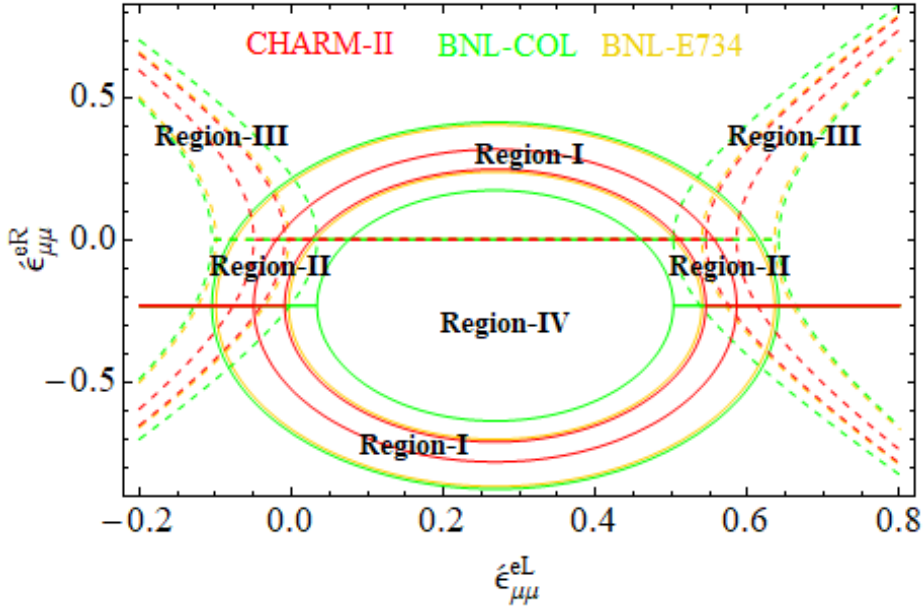


Fig.(9b) Allowed region between ellipse for Imaginary part of  $\epsilon_{ee}^{eR}$ , depends on  $\epsilon_{ee}^{eL}$ . CHARM-II, BNL-COL and BNL-E734 represented by Red, blue and orange color respectively at 90% CL



Fig(9c). Overlapping of Figs (9a and 9b). Region-I is physical allowed region, whereas Region-II is allowed region contain real values of  $\epsilon_{\mu\mu}^{eR}$  from upper 90% CL and imaginary values from lower 90%CL depends on  $\epsilon_{\mu\mu}^{eL}$ . Region-III is complex allowed region of  $\epsilon_{\mu\mu}^{eR}$ .

The overlapping of Fig.(9a and 9b) can be seen in Fig.(9c).

#### IV. MD ANALYSIS OF $\nu_{\alpha e} \rightarrow \nu_{\beta e}$

For Model Dependent (MD) analysis,  $\mathcal{R}_p$  SUSY is selected. Assuming the particle content of the Minimal Supersymmetric Standard Model (MSSM), the most general  $\mathcal{R}_p$  superpotential Eq.(1) involving only the tri-linear couplings. In terms of the component fields (with the sfermion fields characterized by  $\tilde{\phantom{x}}$  sign), the trilinear terms lead to

interaction of the form

$$L_{(R_p)} = \lambda_{ijk} [\tilde{\nu}_{iL} \bar{e}_{kR} e_{jL} + \tilde{e}_{jL} \bar{e}_{kR} \nu_{iL} + \tilde{e}_{kR}^* (\bar{\nu}_{iL})^c e_{jL}] \quad (14)$$

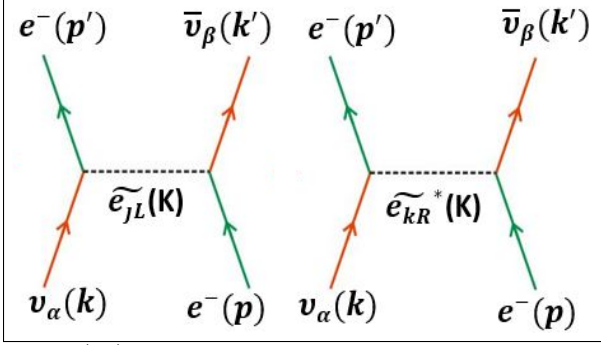


Fig. (10)  $\nu_\alpha e \rightarrow \nu_\beta e$  SUSY feynman diagrams

The relevant terms for process  $\nu_\alpha e \rightarrow \nu_\beta e$  are  $\tilde{e}_{jL} \bar{e}_{kR} \nu_{iL}$  and  $\tilde{e}_{kR}^* (\bar{\nu}_{iL})^c e_{jL}$  can proceed through Feynman diagrams Fig.(10)

The R-parity Lagrangian for interaction of  $\tilde{e}_{jL} \bar{e}_{kR} \nu_{iL}$  and  $\tilde{e}_{kR}^* (\bar{\nu}_{iL})^c e_{jL}$  can be written in Eq.(15) and Eq.(16) respectively

$$L_{R_p}^a = -\frac{8G_F}{\sqrt{2}} A_{\alpha\beta}^{ee} [\bar{\nu}_\beta(k') \gamma_\mu P_L \nu_\alpha(k) \bar{e}(p') \gamma^\mu P_R e(p)] \quad (15)$$

$$L_{R_p}^b = -\frac{8G_F}{\sqrt{2}} B_{\alpha\beta}^{ee} [\bar{\nu}_\beta(k') \gamma_\mu P_L \nu_\alpha(k)] [\bar{e}(p') \gamma^\mu P_L e(p)] \quad (16)$$

where  $A_{\alpha\beta}^{ee} \equiv \frac{\sqrt{2}}{8G_F} \sum_j \frac{\lambda_{\alpha j 1} \lambda_{\beta j 1}^*}{\tilde{m}_{jL}^2}$ ;  $B_{\alpha\beta}^{ee} \equiv \frac{\sqrt{2}}{8G_F} \sum_k \frac{\lambda_{\beta 1 k} \lambda_{\alpha 1 k}^*}{\tilde{m}_{kR}^2}$ .

$\tilde{m}_{jL}$  and  $\tilde{m}_{kR}$  are masses of generation dependent exchanged sleptons. By adding Eq.(15 and 16) we get R-parity effective Lagrangian

$$L_{int(R_p)} = -\frac{8G_F}{\sqrt{2}} [\{\bar{\nu}_\beta(k') \gamma_\mu P_L \nu_\alpha(k)\} \{\bar{e}(p') \gamma^\mu (A_{\alpha\beta}^{ee} P_R + B_{\alpha\beta}^{ee} P_L) e(p)\}] \quad (17)$$

For  $\nu_e e$  elastic scattering  $B_{\alpha\beta}^{ee} \equiv \frac{\sqrt{2}}{8G_F} \sum_k \frac{\lambda_{\beta 1 k} \lambda_{\alpha 1 k}^*}{\tilde{m}_{kR}^2}$  becomes zero due to anti-symmetric nature of  $\lambda_{11k} \lambda_{11k}^*$ . Total cross-section for  $\nu_e e \rightarrow \nu_e e$  and  $\nu_\mu e \rightarrow \nu_\mu e$  are

$$\sigma^{\nu_e} = 4\sigma_o \left[ \left(1 + \frac{g_L}{2}\right)^2 + \frac{1}{3} \left(\frac{g_R}{2} + \frac{1}{\sqrt{2}G_F} \sum_j \frac{|\lambda_{1j1}|^2}{\tilde{m}_{jL}^2}\right)^2 \right] \quad (18)$$

$$\sigma^{\nu_\mu} = 4\sigma_o \left[ \left(\frac{g_L}{2} + \frac{1}{\sqrt{2}G_F} \sum_k \frac{|\lambda_{21k}|^2}{\tilde{m}_{kR}^2}\right)^2 + \frac{1}{3} \left(\frac{g_R}{2} + \frac{1}{\sqrt{2}G_F} \sum_j \frac{|\lambda_{2j1}|^2}{\tilde{m}_{jL}^2}\right)^2 \right] \quad (19)$$

At  $\tilde{m}_{kR} = \tilde{m}_{jL} = 100 GeV$  and using  $\sigma^{\nu_e} = \sigma_{exp}^{\nu_e}$  from LSND experiment, we plot Eq.(18) at 1, 1.8 and 2 upper sigma level shown in Fig.(11). In the Fig.(11) it is clear that limits on  $R_p$  SUSY Model coupling parameter should lie in the interval  $-0.26 \leq \lambda_{1j1} \leq 0.26$ , at  $+1\sigma$  level,  $-0.30 \leq \lambda_{1j1} \leq 0.30$  at  $+1.8\sigma$  level and  $-0.31 \leq \lambda_{1j1} \leq 0.31$  at  $+2\sigma$  level. SM cross-section can be obtain only by setting  $\lambda_{1j1} = 0$ .



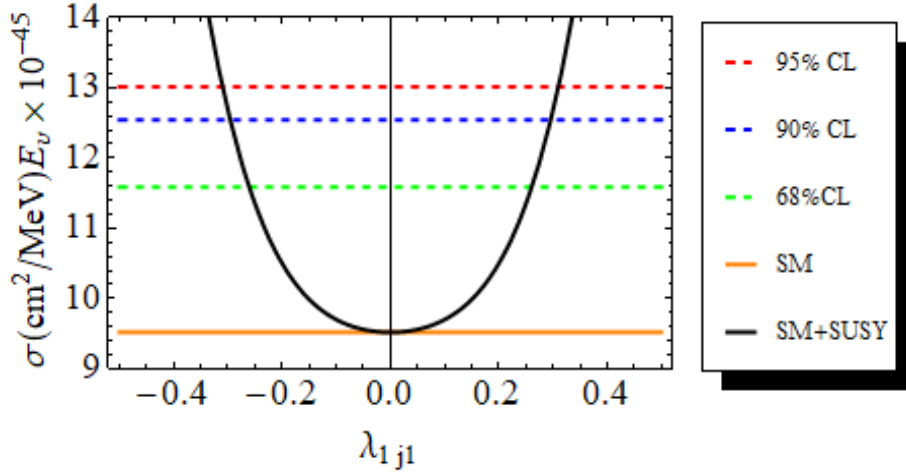


Fig. (11) R-parity violating SUSY model parameter  $\lambda_{1j1}$  upper limits at different C.L, at  $\tilde{m}_{kR} = \tilde{m}_{jL} = 100\text{GeV}$

By rearranging Eq.(19) we get

$$\frac{1}{\sqrt{2}G_F} \sum_j \frac{|\lambda_{2j1}|^2}{\tilde{m}_{jL}^2} = \sqrt{\sqrt{\frac{3\sigma_{\text{exp}}^{\nu\mu}}{4\sigma_o} - 3 \left( \frac{g_L}{2} + \frac{1}{\sqrt{2}G_F} \sum_k \frac{|\lambda_{21k}|^2}{\tilde{m}_{kR}^2} \right)^2} - \frac{g_R}{2}} \quad (20)$$

We analyze eq.(20) by using the experimental values of CHARM-II, BNL-COL and BNL-E734 and obtained the Figs.( 12a, 12b and 12c) that reveal the sensitivity of  $\mathcal{R}_p$  SUSY Model coupling parameters ( $\lambda_{2j1}$  and  $\lambda_{21k}$ ) to each other.

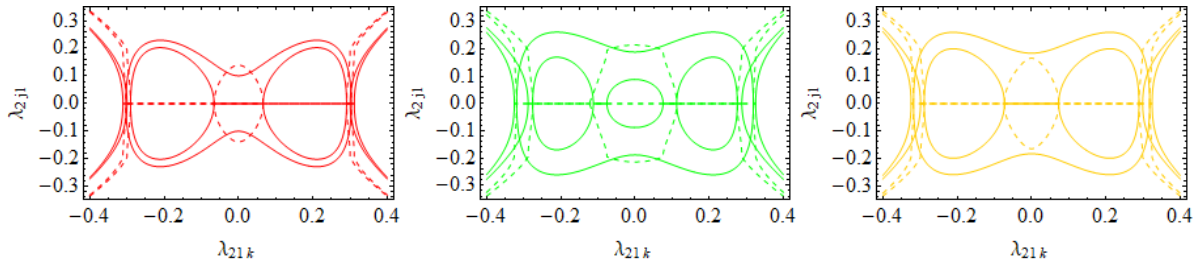


Fig.(12a) Allowed (complex and real) and Disallowed Region for  $\lambda_{2j1}$  depend on  $\lambda_{21k}$  coupling at  $\tilde{m}_{kR} = \tilde{m}_{jL} = 100\text{GeV}$  from CHARM-II experiment at 90%CL. Solid and dotted lines represent real and imaginary values respectively

Fig.(12b) Allowed (complex and real) and Disallowed Region for  $\lambda_{2j1}$  depend on  $\lambda_{21k}$  coupling at  $\tilde{m}_{kR} = \tilde{m}_{jL} = 100\text{GeV}$  from BNL-COL experiment at 90%CL. Solid and dotted lines represent real and imaginary values respectively

Fig.(12c) Allowed (complex and real) and Disallowed Region for  $\lambda_{2j1}$  depend on  $\lambda_{21k}$  coupling at  $\tilde{m}_{kR} = \tilde{m}_{jL} = 100\text{GeV}$  from BNL-E734 experiment at 90%CL. Solid and dotted lines represent real and imaginary values respectively

The combine region wise sensitivity of  $\lambda_{2j1}$  on  $\lambda_{21k}$  for CHARM-II, BNL-COL and BNL-E734 can be seen in Fig.(13)

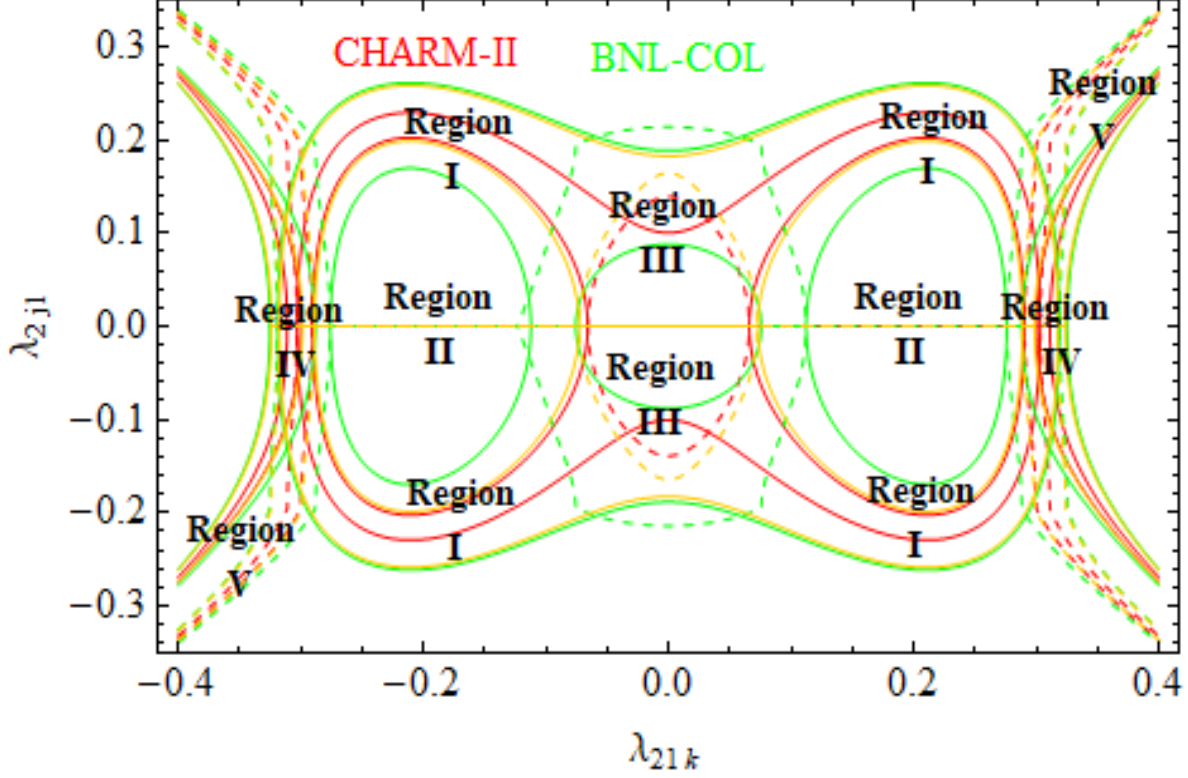


Fig. (13) Physical Allowed and Disallowed Region for  $\lambda_{2j1}$  depend on  $\lambda_{21k}$  coupling at  $\tilde{m}_{kR} = \tilde{m}_{jL} = 100\text{GeV}$  from CHARM-II, BNL-COL and BNL-E734 experiments at 90%CL. Solid and dotted lines represent real and imaginary values respectively

Region-I is real physically allowed for  $\lambda_{2j1}$  depends on  $\lambda_{21k}$ . The Region-III and IV are allowed regions and contain complex value of  $\lambda_{2j1}$  from upper 90%CL and real value from lower 90% CL. The Region-V is allowed and have complex values of  $\lambda_{2j1}$ . The Region-II is only forbidden due to experimental constraints. In literature [53–55], single coupling dominances hypothesis is used for constraining R-parity violating Yukawa coupling which is equivalent to hiding important facts under the rug. Quite misleading.

By direct Comparison of eqs.(9 and 17) we get the relation between MI coupling parameters and R-parity violating SUSY Model coupling parameters.

$$\xi_{\alpha\beta}^{eL} = \frac{1}{\sqrt{2}G_F} \sum_k \frac{\lambda_{\beta 1k} \lambda_{\alpha 1k}^*}{\tilde{m}_{kR}^2} \quad (21)$$

$$\xi_{\alpha\beta}^{eR} = \frac{1}{\sqrt{2}G_F} \sum_j \frac{\lambda_{\alpha j1} \lambda_{\beta j1}^*}{\tilde{m}_{jL}^2} \quad (22)$$

## V. RESULTS AND DISCUSSION

We have performed a complete survey of  $\nu_{\alpha e} \rightarrow \nu_{\beta e}$  scattering and calculate related percentage error. The major contribution in the cross-section of  $\nu_e e$  and  $\nu_{\mu e}$  is found to be coming from SM mentioned in Table-I. Figs.(2, 3, 4 and 5), shows the size of discrepancies between SM and experimental cross-section for the process  $\nu_e e \rightarrow \nu_e e$  and  $\nu_{\mu e} \rightarrow \nu_{\mu e}$  at 68%, 90% and 95% Confidence levels. These discrepancies give us a hint for the possibility of NSI and the size of discrepancies shows available room for NSI. Although the discrepancy between experimental value and SM prediction is very small but due to non-zero masses of neutrinos, we cannot neglect the NSI. The deviation from experimental limits places bounds on new physics(NP) parameters at different error levels. By using advance neutrino experiments i.e. super-beams,  $\beta$ -beams or neutrino factory, we can correctly estimate uncertainties and discover NP within them.

One of the possible explanation of this discrepancy lies in the fact that the neutrinos are treated as massless particles which couple universally with gauge bosons. But the oscillations of neutrinos depict that they carry mass, therefore, coupling must be non-universal. So incorporating the non-universal NSI is a must to reduce the bridge between theory and experiments.

In order to achieve this goal both Model Independent (MI) and Model Dependent (MD) ( R-parity violating SUSY Model), detailed analysis have been performed and relationship between MI and MD parameters is established.

In MI analysis the non-standard interaction is incorporated through non universal flavour diagonal couplings, and analysis is performed involving total cross-section for  $\nu_e e \rightarrow \nu_e e$  and  $\nu_\mu e \rightarrow \nu_\mu e$  as a sub-leading effect.

We discuss the sensitivity of flavour diagonal NSI Yukawa couplings parameters ( $\hat{\epsilon}_{ee}^{eL}, \hat{\epsilon}_{ee}^{eR}$  and  $\hat{\epsilon}_{\mu\mu}^{eL}, \hat{\epsilon}_{\mu\mu}^{eR}$ ) and identify the physically allowed and forbidden regions for these coupling parameters under the experimental constraints of LSND, CHARM-II, BNL-COL and BNL-E734 experimental shown in Figs.(7c and 9c). The sensitivity of  $\hat{\epsilon}_{ee}^{eR}$  on  $\hat{\epsilon}_{ee}^{eL}$  shown in Fig(7c) where Region-I (Rose shaded) is real allowed region for  $\hat{\epsilon}_{ee}^{eR}$ . Region-II (between red and blue dotted lines) is allowed region contain Imaginary part of  $\hat{\epsilon}_{ee}^{eR}$ , and its real part is constant represent by solid blue straight line. Region-III (yellow shaded) is also allowed region contain complex  $\hat{\epsilon}_{ee}^{eR}$  (blue color) from lower 90%CL and real  $\hat{\epsilon}_{ee}^{eR}$  (red color) from upper 90%CL. The sensitivity of  $\hat{\epsilon}_{\mu\mu}^{eR}$  on  $\hat{\epsilon}_{\mu\mu}^{eL}$  shown in Fig(9c) where Region-I is real allowed region for  $\hat{\epsilon}_{\mu\mu}^{eR}$ . Region-II contain complex value of  $\hat{\epsilon}_{\mu\mu}^{eR}$  from lower 90%CL and real value of  $\hat{\epsilon}_{\mu\mu}^{eR}$  from upper 90%CL. The Region-III is complex allowed region for  $\hat{\epsilon}_{\mu\mu}^{eR}$ . The Region-IV is disallowed region.

For MD (R-parity violating SUSY Model) analysis, the most general R-parity violating superpotential is introduced and R-parity violating currents pertaining to the process are also discussed. We have calculated elastic scattering cross-section  $\sigma_{elastic}(SM+R\text{-parity SUSY Model})$  for  $\nu_e e \rightarrow \nu_e e$  and  $\nu_\mu e \rightarrow \nu_\mu e$  in term of NUFD R-parity violating SUSY Model coupling parameters ( $\lambda_{\alpha 1k}, \lambda_{\alpha j1}$ ).

The contribution of  $\lambda_{\alpha 1k}$  becomes zero due to the anti-symmetry present in first two indices and only  $\lambda_{\alpha j1}$  contributes for  $\nu_e e$  elastic scattering. We also plot  $\sigma_{elastic}(SM+R\text{-parity SUSY Model})$  vs  $\lambda_{1j1}$  for  $\nu_e e \rightarrow \nu_e e$  and set the limits  $-0.26 \leq \lambda_{1j1} \leq 0.26$ , at  $+1\sigma$ ,  $-0.30 \leq \lambda_{1j1} \leq 0.30$  at  $+1.8\sigma$  and  $-0.31 \leq \lambda_{1j1} \leq 0.31$  at  $+2\sigma$  level by using LSND experimental value as shown in Fig.(11).

We reveal the sensitivity of  $\hat{R}_p$  SUSY Model coupling parameters ( $\lambda_{2j1}$  and  $\lambda_{21k}$ ) to each other shown in Fig.(13) by using the experimental values of CHARM-II, BNL-COL and BNL-E734. Now the situation is quite different in model dependent ( $\hat{R}_p$  SUSY model) scenario after incorporating propagating particles. The shapes of plots have changed from ellipse to butterfly and thus making the overall picture involving coupling parameters ( $\lambda_{2j1}, \lambda_{21k}$ ) more clear as shown in Figs.(12a, 12b, 12c and 13). In Fig.(13) the Region-I is the physical real allowed region for coupling parameters ( $\lambda_{2j1}, \lambda_{21k}$ ), Region-II is disallowed region. Region-III and IV are allowed regions, contain Imaginary and real value of  $\lambda_{2j1}$  from lower and upper 90%CL respectively. The Region-V is allowed complex region for coupling parameter  $\lambda_{2j1}$ .

We have also developed the relation between MI coupling parameters ( $\hat{\epsilon}_{ee}^{eL}, \hat{\epsilon}_{ee}^{eR}$ ) and R-parity violating SUSY Model coupling parameters ( $\lambda_{\alpha 1k}, \lambda_{\alpha j1}$ ) in term of Fermi coupling constant  $G_F$  and mass of SUSY propagator(21 and 22).

The analysis provides physically allowed and forbidden regions rather than just limits/bounds to non- standard neutrino interactions (NSNI) in truly MI and MD way. We have also demonstrated that working within the discrepancies and using approximations (means hiding certain facts) has great impact on particle physics phenomenology. Hence, this analysis highlights the importance of NSIs in precision measurements.

- [1] M. Deniz, et al., [TEXONO Collaboration], Phys. Rev. D 82 (2010) 033004.
- [2] L.B Auerbach, et al., [LSND Collaboration], Phys. Rev. D 63 (2001) 11.
- [3] S. Davidson, C. Pena-Garay, N. Rius, and A. Santamaria, JHEP 03 (2003) 011, [arXiv:hep-ph/0302093 v2].
- [4] W. N. Cottingham and D. A. Greenwood, "An Introduction to the Standard Model of Particle Physics", (2nd ed), Cambridge University Press (2007).
- [5] G. Kane, "Modern Elementary Particle Physics", Addison-Wesley Publishing Company (1993).
- [6] Q. R. Ahmad et al., [SNO Collaboration], Phys. Rev. Lett. 89 (2002) 011301.
- [7] Y. Fukuda, et al., [Super-Kamiokande Collaboration], Phys. Rev. Lett. 81 (1998) 1562.
- [8] T. Toshito. [Super-Kamiokande Collaboration], arXiv:hep-ex/0105023.
- [9] S. M. Bilenky, and C. Giunti, Inter. Journal. Mod. Phys. A 16 (2001) 3931.
- [10] Y. Wang and Z.Z. Xing, [arXiv:1504.06155v1] and references therein.
- [11] T. Ohlsson., Rep. Prog. Phys. 76 (2013) 044201, and references therein.
- [12] M. Deniz, et al., [TEXONO Collaboration], Phys. Rev. D 81 (2010) 072001.
- [13] G. Ciezarek, et al., Nature 546 (2017) 227.

- [14] F. Archilli et al., *Nature* 546 (2017) 221.
- [15] A. Zee, *Phys. Lett. B* 161 (1985) 141.
- [16] M. Fukugita and T. Yanagida, *Phys. Lett. B* 206 (1988) 93.
- [17] X. G. He, G. C. Joshi, H. Lew and R. R. Volkas, *Phys. Rev. D* 43 (1991) 22.
- [18] X. G. He, G. C. Joshi, H. Lew and R. R. Volkas, *Phys. Rev. D* 44 (1991) 2118.
- [19] C. T. Hill, *Phys. Lett. B* 345 (1995) 483, [arXiv:hep-ph/9411426].
- [20] R. S. Chivukula, B. A. Dobrescu and J. Terning, *Phys. Lett. B* 353 (1995) 289, [arXiv:hep-ph/9503203].
- [21] K. D. Lane and E. Eichten, *Phys. Lett. B* 352 (1995) 382, [arXiv:hep-ph/9503433].
- [22] G. Buchalla, G. Burdman, C. T. Hill, and D. Kominis, *Phys. Rev. D* 53 (1996) 5185, [arXiv:hep-ph/9510376].
- [23] K. D. Lane, *Phys. Rev. D* 54 (1996) 2204, [arXiv:hep-ph/9602221].
- [24] E. Ma, *Phys. Lett. B* 433 (1998) 74, [arXiv:hep-ph/9709474].
- [25] E. Ma and U. Sarkar, *Phys. Lett. B* 439 (1998) 95, [arXiv:hep-ph/9807307].
- [26] E. Ma, D. P. Roy and U. Sarkar, *Phys. Lett. B* 444 (1998) 391, [arXiv:hep-ph/9810309].
- [27] E. Ma and D. P. Roy, *Phys. Rev. D* 58 (1998) 095005, [arXiv:hep-ph/9806210].
- [28] E. Ma and D. P. Roy, *Phys. Rev. D* 59 (1999) 097702, [arXiv:hep-ph/9811266].
- [29] K. D. Lane, *Phys. Lett. B* 433 (1998) 96, [arXiv:hep-ph/9805254].
- [30] W. Loinaz and T. Takeuchi, *Phys. Rev. D* 60 (1999) 115008, [arXiv:hep-ph/9903362].
- [31] L. N. Chang, O. Lebedev, W. Loinaz, and T. Takeuchi, *Phys. Rev. D* 63 (2001) 074013, [arXiv:hep-ph/0010118].
- [32] P. B. Pal and U. Sarkar, *Phys. Lett. B* 573 (2003) 147, [arXiv:hep-ph/0306088].
- [33] M. Honda, et al., [arXiv:hep-ph/07074545].
- [34] F. F. Deppisch, et al., *Phys. Lett. B* 762 (2016) 432.
- [35] L. A. Sanchez, W. A. Ponce, and R. Martinez, *Phys. Rev. D* 64 (2001) 075013.
- [36] J. G. Ferreira, et. al., *Phys. Rev. D* 84 (2011) 095019.
- [37] F. Pisano and V. Pleitez., *Phys. Rev. D* 46 (1992) 1.
- [38] L. A. Sánchez, W. A. Ponce, and R. Martinez., *Phys. Rev. D* 67 (2001) 075013, [arXiv:hep-ph/0103244].
- [39] W. A. Ponce, J. B. Florez, and L. A. Sánchez., *Int. J. Mod. Phys. A* 17 (2002) 643.
- [40] C. Promberger, S. Schatt, and F. Schwab, *Phys. Rev. D* 75 (2007) 115007.
- [41] E. M. Sessolo, F. Tahir, and D. W. McKay, *Phys. Rev. D* 79 (2009) 115010.
- [42] S. Raychaudhuri., *hep-ph/9905576*.
- [43] F. Tahir, M. Sadiq, M. Anwar Mughal, and K. Ahmed, *Phys. Rev. Lett. B* 439 (1998) 316.
- [44] F. Tahir, M. Anwar Mughal, and K. Ahmed, *Europhys. Lett.* 53 (2001) 29.
- [45] F. Tahir, M. Anwar Mughal, and K. Ahmed, *Europhys. Lett.* 54 (2001) 05.
- [46] V. Bednyakov, et al., *hep-ph/9904414*.
- [47] P. Vilain et al., (CHARM II Collaboration), *Phys. Lett. B* 335 (1994) 246.
- [48] L.A. Ahrens et al., *Phys. Rev. D.* 41 (1990) 3297.
- [49] N.J. Baker et al., *Phys. Rev. D* 40 (1989) 2753.
- [50] G. Radell and R. Beyer, *Mod. Phys. Lett. A* 08 (1993) 1067.
- [51] B. Kayser, E. Fischbach, S. P. Rosen, and H. Spivack, *Phys. Rev. D.* 20 (1979) 87.
- [52] R. N. Mohapatra, "Massive Neutrinos in Physics and Astrophysics", (3rd ed), World Scientific Publishing (2002).
- [53] V. Barger, G.F. Giudice and T. Han, *Phys. Rev. D* 40 (1989) 2987.
- [54] Herbi Dreiner, [arXiv:hep-ph/9707435].
- [55] R. Barbier et al., *Phys. Rept.* 420 (2005), [arXiv:hep-ph/0406039] and references therein

$\epsilon_{ee}^{eL}$	Real limits on $\epsilon_{ee}^{eR}$	
-1.3	$-1.332 \leq \epsilon_{ee}^{eR} \leq -0.832$	$0.3696 \leq \epsilon_{ee}^{eR} \leq 0.868$
-1.2	$-1.465 \leq \epsilon_{ee}^{eR} \leq -1.051$	$0.589 \leq \epsilon_{ee}^{eR} \leq 1.003$
-1.1	$-1.563 \leq \epsilon_{ee}^{eR} \leq -1.192$	$0.730 \leq \epsilon_{ee}^{eR} \leq 1.101$
-1.0	$-1.633 \leq \epsilon_{ee}^{eR} \leq -1.287$	$0.825 \leq \epsilon_{ee}^{eR} \leq 1.171$
-0.9	$-1.679 \leq \epsilon_{ee}^{eR} \leq -1.347$	$0.885 \leq \epsilon_{ee}^{eR} \leq 1.217$
-0.8	$-1.704 \leq \epsilon_{ee}^{eR} \leq -1.379$	$0.917 \leq \epsilon_{ee}^{eR} \leq 1.242$
-0.7	$-1.707 \leq \epsilon_{ee}^{eR} \leq -1.384$	$0.922 \leq \epsilon_{ee}^{eR} \leq 1.246$
-0.6	$-1.691 \leq \epsilon_{ee}^{eR} \leq -1.363$	$0.901 \leq \epsilon_{ee}^{eR} \leq 1.229$
-0.5	$-1.653 \leq \epsilon_{ee}^{eR} \leq -1.313$	$0.852 \leq \epsilon_{ee}^{eR} \leq 1.191$
-0.4	$-1.592 \leq \epsilon_{ee}^{eR} \leq -1.233$	$0.771 \leq \epsilon_{ee}^{eR} \leq 1.131$
-0.3	$-1.506 \leq \epsilon_{ee}^{eR} \leq -1.111$	$0.649 \leq \epsilon_{ee}^{eR} \leq 1.044$
-0.2	$-1.387 \leq \epsilon_{ee}^{eR} \leq -0.928$	$0.466 \leq \epsilon_{ee}^{eR} \leq 0.925$
-0.1	$-1.225 \leq \epsilon_{ee}^{eR} \leq -0.602$	$0.120 \leq \epsilon_{ee}^{eR} \leq 0.763$

TABLE I: Real Limits from Region-I

$\epsilon_{ee}^{eL}$	Real and complex Limits on $\epsilon_{ee}^{eR}$	
-1.5	$-0.870 \leq \epsilon_{ee}^{eR} \leq 0.408$	$-0.231 - 0.665i \leq \epsilon_{ee}^{eR} \leq -0.231 + 0.665i$
-1.4	$-1.148 \leq \epsilon_{ee}^{eR} \leq 0.686$	$-0.231 - 0.103i \leq \epsilon_{ee}^{eR} \leq -0.231 + 0.103i$
0.0	$-0.993 \leq \epsilon_{ee}^{eR} \leq 0.531$	$-0.231 - 0.521i \leq \epsilon_{ee}^{eR} \leq -0.231 + 0.521i$
0.1	$-0.565 \leq \epsilon_{ee}^{eR} \leq 0.103$	$-0.231 - 0.860i \leq \epsilon_{ee}^{eR} \leq -0.231 + 0.860i$

TABLE II: Real and complex Limits from Region-II

$\epsilon_{ee}^{eL}$	Complex Limits on $\epsilon_{ee}^{eR}$	
-2.0	$-0.231 - 1.627i \geq \epsilon_{ee}^{eR} \geq -0.231 - 1.871i$	$-0.231 + 1.627i \leq \epsilon_{ee}^{eR} \leq -0.231 + 1.871i$
-1.9	$-0.231 - 1.384i \geq \epsilon_{ee}^{eR} \geq -0.231 - 1.664i$	$-0.231 + 1.384i \leq \epsilon_{ee}^{eR} \leq -0.231 + 1.664i$
-1.8	$-0.231 - 1.116i \geq \epsilon_{ee}^{eR} \geq -0.231 - 1.448i$	$-0.231 + 1.116i \leq \epsilon_{ee}^{eR} \leq -0.231 + 1.448i$
-1.7	$-0.231 - 0.796i \geq \epsilon_{ee}^{eR} \geq -0.231 - 1.219i$	$-0.231 + 0.796i \leq \epsilon_{ee}^{eR} \leq -0.231 + 1.219i$
-1.6	$-0.231 - 0.287i \geq \epsilon_{ee}^{eR} \geq -0.231 - 0.966i$	$-0.231 + 0.287i \leq \epsilon_{ee}^{eR} \leq -0.231 + 0.966i$
0.2	$-0.231 - 0.646i \geq \epsilon_{ee}^{eR} \geq -0.231 - 1.126i$	$-0.231 + 0.646i \leq \epsilon_{ee}^{eR} \leq -0.231 + 1.126i$
0.3	$-0.231 - 1.003i \geq \epsilon_{ee}^{eR} \geq -0.231 - 1.363i$	$-0.231 + 1.003i \leq \epsilon_{ee}^{eR} \leq -0.231 + 1.363i$
0.4	$-0.231 - 1.286i \geq \epsilon_{ee}^{eR} \geq -0.231 - 1.583i$	$-0.231 + 1.286i \leq \epsilon_{ee}^{eR} \leq -0.231 + 1.583i$
0.5	$-0.231 - 1.537i \geq \epsilon_{ee}^{eR} \geq -0.231 - 1.793i$	$-0.231 + 1.537i \leq \epsilon_{ee}^{eR} \leq -0.231 + 1.793i$

TABLE III: Complex Limits from Region-III

$\epsilon_{ee}^{eR}$	Real limits on $\epsilon_{ee}^{eL}$	
-1.3	$-1.31988 \leq \epsilon_{ee}^{eL} \leq -0.982153$	$-0.479847 \leq \epsilon_{ee}^{eL} \leq -0.142124$
-1.2	$-1.37498 \leq \epsilon_{ee}^{eL} \leq -1.09295$	$-0.369045 \leq \epsilon_{ee}^{eL} \leq -0.0870214$
-1.1	$-1.42091 \leq \epsilon_{ee}^{eL} \leq -1.1695$	$-0.292505 \leq \epsilon_{ee}^{eL} \leq -0.0410906$
-1.0	$-1.45941 \leq \epsilon_{ee}^{eL} \leq -1.22787$	$-0.234132 \leq \epsilon_{ee}^{eL} \leq -0.00259418$
-0.9	$-1.4916 \leq \epsilon_{ee}^{eL} \leq -1.27397$	$-0.188035 \leq \epsilon_{ee}^{eL} \leq 0.0295974$
-0.8	$-1.51826 \leq \epsilon_{ee}^{eL} \leq -1.31072$	$-0.151278 \leq \epsilon_{ee}^{eL} \leq 0.0562579$
-0.7	$-1.53993 \leq \epsilon_{ee}^{eL} \leq -1.33983$	$-0.122167 \leq \epsilon_{ee}^{eL} \leq 0.0779345$
-0.6	$-1.55702 \leq \epsilon_{ee}^{eL} \leq -1.36236$	$-0.0996432 \leq \epsilon_{ee}^{eL} \leq 0.0950196$
-0.5	$-1.56979 \leq \epsilon_{ee}^{eL} \leq -1.37898$	$-0.08302 \leq \epsilon_{ee}^{eL} \leq 0.107794$
-0.4	$-1.57845 \leq \epsilon_{ee}^{eL} \leq -1.39015$	$-0.0718505 \leq \epsilon_{ee}^{eL} \leq 0.116452$
-0.3	$-1.58312 \leq \epsilon_{ee}^{eL} \leq -1.39614$	$-0.0658599 \leq \epsilon_{ee}^{eL} \leq 0.12112$
-0.2	$-1.58386 \leq \epsilon_{ee}^{eL} \leq -1.39709$	$-0.0649084 \leq \epsilon_{ee}^{eL} \leq 0.121863$
-0.1	$-1.58069 \leq \epsilon_{ee}^{eL} \leq -1.39303$	$-0.0689743 \leq \epsilon_{ee}^{eL} \leq 0.118691$
0.0	$-1.57356 \leq \epsilon_{ee}^{eL} \leq -1.38385$	$-0.0781514 \leq \epsilon_{ee}^{eL} \leq 0.111561$
0.1	$-1.56237 \leq \epsilon_{ee}^{eL} \leq -1.36934$	$-0.0926599 \leq \epsilon_{ee}^{eL} \leq 0.100369$
0.2	$-1.54695 \leq \epsilon_{ee}^{eL} \leq -1.34912$	$-0.112875 \leq \epsilon_{ee}^{eL} \leq 0.0849504$
0.3	$-1.52706 \leq \epsilon_{ee}^{eL} \leq -1.32262$	$-0.139382 \leq \epsilon_{ee}^{eL} \leq 0.065058$
0.4	$-1.50235 \leq \epsilon_{ee}^{eL} \leq -1.28892$	$-0.173077 \leq \epsilon_{ee}^{eL} \leq 0.0403463$
0.5	$-1.47233 \leq \epsilon_{ee}^{eL} \leq -1.24663$	$-0.215366 \leq \epsilon_{ee}^{eL} \leq 0.0103333$
0.6	$-1.43634 \leq \epsilon_{ee}^{eL} \leq -1.1934$	$-0.268603 \leq \epsilon_{ee}^{eL} \leq -0.0256573$
0.7	$-1.3934 \leq \epsilon_{ee}^{eL} \leq -1.1248$	$-0.337201 \leq \epsilon_{ee}^{eL} \leq -0.068599$
0.8	$-1.34204 \leq \epsilon_{ee}^{eL} \leq -1.03046$	$-0.431537 \leq \epsilon_{ee}^{eL} \leq -0.119956$
0.9	$-1.27992 \leq \epsilon_{ee}^{eL} \leq -0.863708$	$-0.598292 \leq \epsilon_{ee}^{eL} \leq -0.182084$

TABLE IV: Real Limits from Region-I

$\epsilon_{ee}^{eR}$	Real and Complex Limits on $\epsilon_{ee}^{eL}$	
-1.7	$-0.822515 \leq \epsilon_{ee}^{eR} \leq -0.639485$	$-0.731 - 0.524711i \leq \epsilon_{ee}^{eR} \leq -0.731 + 0.524711i$
-1.6	$-1.0519 \leq \epsilon_{ee}^{eR} \leq -0.410103$	$-0.731 - 0.425114i \leq \epsilon_{ee}^{eR} \leq -0.731 + 0.425114i$
-1.5	$-1.16793 \leq \epsilon_{ee}^{eR} \leq -0.294069$	$-0.731 - 0.304612i \leq \epsilon_{ee}^{eR} \leq -0.731 + 0.304612i$
-1.4	$-1.2527 \leq \epsilon_{ee}^{eR} \leq -0.209296$	$-0.731 - 0.10734i \leq \epsilon_{ee}^{eR} \leq -0.731 + 0.10734i$
1.0	$-1.20278 \leq \epsilon_{ee}^{eR} \leq -0.259221$	$-0.731 - 0.247229i \leq \epsilon_{ee}^{eR} \leq -0.731 + 0.247229i$
1.1	$-1.10137 \leq \epsilon_{ee}^{eR} \leq -0.360629$	$-0.731 - 0.382782i \leq \epsilon_{ee}^{eR} \leq -0.731 + 0.382782i$
1.2	$-0.943387 \leq \epsilon_{ee}^{eR} \leq -0.518613$	$-0.731 - 0.488455i \leq \epsilon_{ee}^{eR} \leq -0.731 + 0.488455i$

TABLE V: Real and Complex Limits from Region-II

$\epsilon_{ee}^{eR}$	Complex Limits on $\epsilon_{ee}^{eL}$	
-2.0	$-0.731 - 0.77403i \leq \epsilon_{ee}^{eR} \leq -0.731 - 0.561627i$	$-0.731 + 0.561627i \leq \epsilon_{ee}^{eR} \leq -0.731 + 0.77403i$
-1.9	$-0.731 - 0.696076i \leq \epsilon_{ee}^{eR} \leq -0.731 - 0.448135i$	$-0.731 + 0.448135i \leq \epsilon_{ee}^{eR} \leq -0.731 + 0.696076i$
-1.8	$-0.731 - 0.613668i \leq \epsilon_{ee}^{eR} \leq -0.731 - 0.304781i$	$-0.731 + 0.304781i \leq \epsilon_{ee}^{eR} \leq -0.731 + 0.613668i$
1.3	$-0.731 - 0.580794i \leq \epsilon_{ee}^{eR} \leq -0.731 - 0.231571i$	$-0.731 + 0.231571i \leq \epsilon_{ee}^{eR} \leq -0.731 + 0.580794i$
1.4	$-0.731 - 0.665374i \leq \epsilon_{ee}^{eR} \leq -0.731 - 0.398779i$	$-0.731 + 0.398779i \leq \epsilon_{ee}^{eR} \leq -0.731 + 0.665374i$
1.5	$-0.731 - 0.744841i \leq \epsilon_{ee}^{eR} \leq -0.731 - 0.520665i$	$-0.731 + 0.520665i \leq \epsilon_{ee}^{eR} \leq -0.731 + 0.744841i$
1.6	$-0.731 - 0.820684i \leq \epsilon_{ee}^{eR} \leq -0.731 - 0.62436i$	$-0.731 + 0.62436i \leq \epsilon_{ee}^{eR} \leq -0.731 + 0.820684i$

TABLE VI: Complex Limits from Region-III